

Spin polarization in a T-shape conductor induced by strong Rashba spin-orbit coupling

Masayuki Yamamoto¹, Tomi Ohtsuki² and Bernhard Kramer¹

¹ *I.Institut für Theoretische Physik, Universität Hamburg,
Jungiusstraße 9, 20355 Hamburg, Germany*

² *Department of Physics, Sophia University,
Kioi-cho 7-1, Chiyoda-ku, Tokyo 102-8554, Japan*

(Dated: September 11, 2018)

Abstract

We investigate numerically the spin polarization of the current in the presence of Rashba spin-orbit interaction in a T-shaped conductor proposed by A.A. Kiselev and K.W. Kim (Appl. Phys. Lett. **78** 775 (2001)). The recursive Green function method is used to calculate the three terminal spin dependent transmission probabilities. We focus on single-channel transport and show that the spin polarization becomes nearly 100 % with a conductance close to e^2/h for sufficiently strong spin-orbit coupling. This is interpreted by the fact that electrons with opposite spin states are deflected into an opposite terminal by the spin dependent Lorentz force. The influence of the disorder on the predicted effect is also discussed. Cases for multi-channel transport are studied in connection with experiments.

PACS numbers:

I. INTRODUCTION

Recently, spin-dependent electronic transport is attracting considerable attention because of possible applications to spintronics [1, 2]. Many of the proposals for two dimensional (2D) spintronic devices are based on the presence of spin-orbit coupling in the 2D electron system (2DES) semiconductor heterostructure. There are two types of spin-orbit coupling terms in such systems. One is the so-called Dresselhaus term which originates from the inversion asymmetry of the zinc-blende structure [3]. The other is described by the Rashba Hamiltonian,

$$\mathcal{H}_R = \frac{\alpha}{\hbar}(\sigma_x p_y - \sigma_y p_x) \quad (1)$$

where α denotes the strength of spin-orbit coupling, σ_i and p_i ($i = x, y$) are the Pauli matrices and the components of the momentum, respectively. The Rashba mechanism is due to the effective electric field originating from the asymmetry of the potential confining the 2DES [4, 5].

It is well known that the Rashba term dominates in narrow-gap semiconductors while the Dresselhaus term is dominant in wide-gap systems [6]. Since the strength of the Rashba term can be controlled via external gates [7, 8], 2DESs with Rashba spin-orbit interaction have become most promising for spintronic applications.

In order to realize such devices, one needs spin polarized electrons in the semiconductor inversion layer. Most straightforwardly, one could generate spin polarized electrons by attaching ferromagnetic metallic contacts to the 2DES and by injecting a current [9]. However, it has been found that in practice the efficiency of the spin injection from a ferromagnet into a semiconductor is very poor because of the conductivity mismatch [10]. Thus, alternative methods have to be invented. Since strong spin-orbit scattering can lead to spatially inhomogeneous spin polarization [11] the generation of spin polarized electrons via spin-orbit coupling is in principle possible.

In this paper we consider a conductor with a T-shape structure with Rashba spin-orbit coupling as originally proposed by Kiselev and Kim [12]. For relatively small strength of the spin-orbit coupling, these authors have obtained high spin polarization. However, the corresponding conductance has been found to be very small. This problem of the small conductance has been eventually overcome by considering a ring-shape electron resonator [13]. It has also been reported that spin accumulation occurs for considerably strong spin-

orbit coupling in a quasi-1D wire [14].

In both of the above cases, electron transport in the lowest subband (single-channel transport) has mainly been considered. Due to the self-duality of scattering matrix [15] for the system with spin-orbit interaction, no spin polarization of the current can be obtained for single-channel transport in two-terminal devices. Therefore, one has to consider at least a conductor with three terminals. The single-channel limit seems to be ideal because one can completely suppress the effect of the D'yakonov-Perel' relaxation, which is the major spin relaxation mechanism in such systems [16, 17, 18, 19].

We will show in this paper that the amplitude of the spin polarization becomes almost perfect with only very little loss of the conductance if the spin-orbit interaction is sufficiently strong. We argue that the predicted effect should be experimentally accessible in InAs.

In the next section, we describe the model system to be investigated numerically. We use the Ando tight-binding Hamiltonian with Rashba coupling in the off-diagonal matrix elements [20]. In Sec. III, the results for the dependence of the polarization on the energy and the strength of spin-orbit coupling are presented. The amplitude of spin polarization is shown to depend on the ratio between the π -phase spin precession length and the width of the quantum wires of the T-shape conductor. In Sec. IV, we discuss the origin of the polarization by investigating the spin states of the wave function. We show that the propagating electrons are deflected at the junction by “Lorentz force” due to the spin-orbit induced effective magnetic field proportional to the z -component of the spin state. The effects of disorder and other channels are also investigated. The final section is devoted to the summary of this paper and the discussion for experimental realization.

II. THE MODEL

We consider the T-shape conductor shown in Fig.1 in the presence of Rashba spin-orbit coupling. The sample region is connected to three electron reservoirs by ideal leads. Electron current is injected into the sample from the reservoir 1 and goes to reservoirs 2 or 3. At small voltages, the currents I_{21} and I_{31} from reservoir 1 to reservoirs 2 and 3, respectively, are proportional to the conductances G^{21} and G^{31} .

The Rashba spin-orbit coupling can be described in the tight-binding language by the

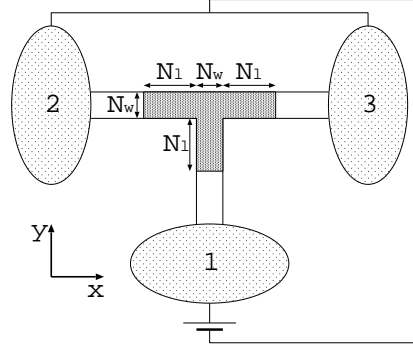


FIG. 1: Schematic view of the T-shaped conductor. Current injected from reservoir 1 can go to reservoirs 2 or 3. Shaded: regions with non-vanishing spin-orbit coupling; parameters: $N_w = 10a$ and $N_l = 20a$ with a lattice spacing of tight-binding model.

Ando Hamiltonian [20],

$$\mathcal{H} = \sum_{i,\sigma} W_i c_{i\sigma}^\dagger c_{i\sigma} - \sum_{\langle i,j \rangle, \sigma, \sigma'} V_{i\sigma, j\sigma'} c_{i\sigma}^\dagger c_{j\sigma'}, \quad (2)$$

where

$$V_{i,i+\hat{x}} = V_0 \begin{pmatrix} \cos \theta & -\sin \theta \\ \sin \theta & \cos \theta \end{pmatrix}, \quad (3)$$

and

$$V_{i,i+\hat{y}} = V_0 \begin{pmatrix} \cos \theta & i \sin \theta \\ i \sin \theta & \cos \theta \end{pmatrix}. \quad (4)$$

Here, $c_{i\sigma}^\dagger (c_{i\sigma})$ denotes the creation (annihilation) operator of an electron on site i with spin σ , W_i the random potential on the site i distributed uniformly in $[-W/2, W/2]$, and $V_{i,i+\hat{x}} (V_{i,i+\hat{y}})$ the hopping matrix elements in x -(y -) directions. The hopping is restricted to nearest neighbours. The hopping energy $V_0 = \hbar^2/2m^*a^2$, where m^* is the effective electron mass and a the tight-binding lattice spacing, is taken as the unit of the energy. The parameter θ represents the strength of the spin-orbit coupling and is related to Rashba coupling α by

$$\alpha \simeq 2\theta V_0 a \quad (\text{for } \theta \ll 1). \quad (5)$$

The conductance between reservoirs J to I [21] and the corresponding spin polarization are defined by

$$G^{IJ} = G_0 \text{Tr } t_{IJ}^\dagger t_{IJ}, \quad (6)$$

and

$$P_k^{IJ} = \frac{\text{Tr}t_{IJ}^\dagger \sigma_k t_{IJ}}{\text{Tr}t_{IJ}^\dagger t_{IJ}} \quad (k = x, y, z), \quad (7)$$

with the conductance quantum $G_0 \equiv e^2/h$, t_{IJ} denoting the transmission matrix from reservoirs J to I . Below, we will focus on the transport between reservoirs 1 and 2. Transport between reservoirs 1 and 3 can trivially be deduced via current conservation and the symmetry of the system. We calculate the amplitude of the total spin polarization defined by

$$|\mathbf{P}| = (P_x^2 + P_y^2 + P_z^2)^{1/2}, \quad (8)$$

instead of considering only the z -component.

As described in detail in Appendix A, we can obtain the transmission coefficient $t_{\mu\nu}^{IJ}$ for the incident channel ν with velocity v_ν in the probe J and out-going channel μ with velocity v_μ in the probe I as [22]

$$t_{\mu\nu}^{IJ} = \left(\frac{v_\mu}{v_\nu} \right)^{1/2} [-(U^I)^{-1} \hat{G}^{IJ} U^J \{(\Lambda^J)^{-1} - \Lambda^J\}]_{\mu\nu} \quad (9)$$

where \hat{G}^{IJ} is Green function corresponding to the transport from the probe J to I . Λ^J contains only diagonal elements, $\Lambda^J(i, j) = \lambda_i^J \cdot \delta_{ij}$, where λ_i^J is the i -th eigenvalue of the transfer matrix for an ideal region in the probe J and $U^{I(J)}$ consists of the set of eigenfunctions for $\{\lambda_i^{I(J)}\}$.

III. RESULTS

Using the recursive Green function method, we calculate the amplitude of the spin polarization. For the system size we assume $N_w = 10a$ and $N_l = 20a$. We first consider an clean system ($W = 0$).

Figure 2 shows the dependence of the conductance and the spin polarization on the Fermi energy E for weak and strong spin-orbit couplings. We consider the energy region for single-channel transport. For weaker spin-orbit coupling ($\theta = 0.02\pi$), high spin polarization is obtained for energies just before the second channel opens ($E \simeq -3.68V_0$). The corresponding conductance is small as compared to G_0 [12]. Almost perfect polarization is obtained together with a conductance close to G_0 for stronger spin-orbit coupling ($\theta = 0.06\pi$). Here, the polarization is almost insensitive to the energy except near the band edge.

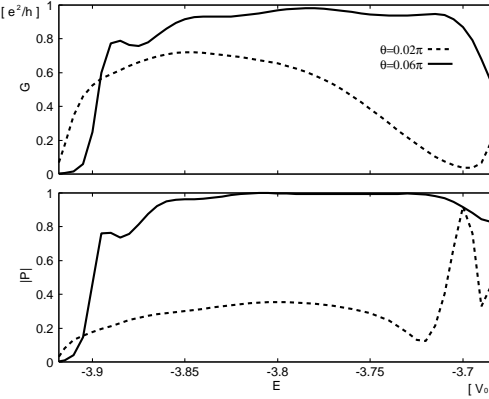


FIG. 2: Conductance G and spin polarization $|P|$ as functions of the Fermi energy E in the region of single-channel transport. Almost 100% polarization is obtained together with $G \approx G_0$ for stronger spin-orbit coupling ($\theta = 0.06\pi$). For $\theta = 0.02\pi$ high polarization is obtained only at energies just before the second channel opens.

Figure 3 shows the dependence of the conductance and the spin polarization on the strength of spin-orbit coupling at energy $E = -3.8V_0$. With the increase of the strength of spin-orbit coupling, P_y also increases monotonically while P_x and P_z oscillate. We also note that the conductance increases together with the amplitude of the polarization. Due to the symmetry of the T-shaped conductor, the current into reservoir 3 has the same polarization in the direction of y but opposite polarizations in x - and z -directions [12].

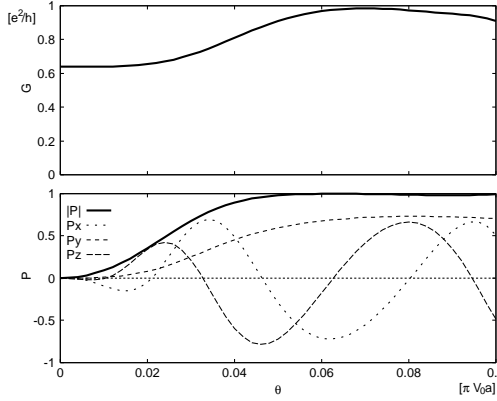


FIG. 3: Conductance G and spin polarization P_k in the directions of $k = x, y, z$ as functions of the strength of spin-orbit coupling θ for $E = -3.8V_0$; P_y increases monotonically with increasing θ while P_x and P_z oscillate.

What are the conditions for achieving almost perfect polarization? We define the π -phase

spin precession length $L_{\text{so}}(|P|, N_w) = \pi a / 2\theta(|P|, N_w)$ where $\theta(|P|, N_w)$ is the spin-orbit coupling strength giving rise to the polarization $|P|$ for the width N_w . From the plot $L_{\text{so}}(|P|, N_w)$ as a function of the width of the system N_w (Fig. 4) one concludes that $L_{\text{so}}(|P|, N_w)$ is almost linear in N_w and high polarization, $|P| > 0.99$, is achieved for $L_{\text{so}}(|P|, N_w) < N_w$. On the other hand, no dependence on the length of the leads (N_l) is observed as shown in Fig. 5.

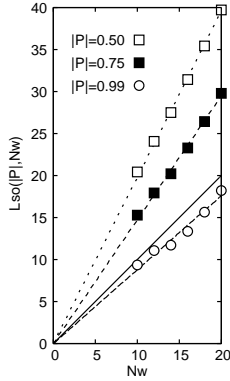


FIG. 4: The spin precession lengths L_{so} for $|P| = 0.5, 0.75, 0.99$ as functions of the width of the wires N_w . Energy is set to be the middle of lowest and first excited subband, e.g., $E = -3.8V_0$ for $N_w = 10$. The polarization becomes almost perfect if the spin precession length becomes shorter than the wire width, $L_{\text{so}}(|P|, N_w) = \pi a / 2\theta(|P|, N_w) < N_w$. Solid line: $L_{\text{so}}(|P|, N_w) = N_w$ corresponding to $|P| \simeq 0.97$.

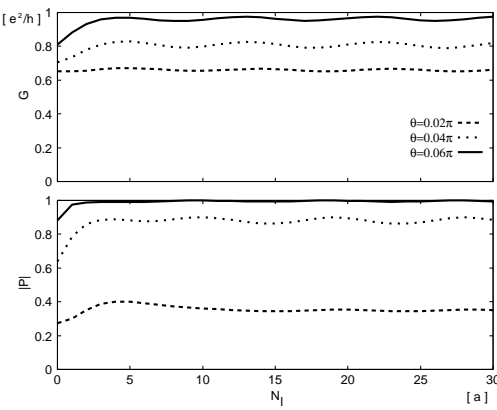


FIG. 5: Conductance G and spin polarization $|P|$ as functions of the wire length N_l for several strengths of the spin-orbit coupling at $E = -3.8V_0$. The polarizations are insensitive to the length of leads except for very short length.

IV. DISCUSSION

It is well known that the spin-orbit interaction is the origin of the anomalous Hall effect in ferromagnetic materials [23]. This is because the spin-orbit coupling affects polarized conduction electrons as a spin-dependent effective magnetic field. In this section, we investigate the spin wave function and show that propagating electrons are deflected at the junction by the Lorentz force due to the spin-orbit induced effective magnetic field proportional to the z -component of the spin [23, 24, 25]. We also investigate the effect of disorder and the influence of other transport channels.

A. Spin-orbit induced effective magnetic field

A convenient way of deriving the effective magnetic field is to estimate the flux per plaquette from the Aharonov–Bohm phase. Let an electron initially be at (i, j) . When it hops from (i, j) to $(i + \hat{x}, j)$ to $(i + \hat{x}, j + \hat{y})$ according to Eqs. (3) and (4), the SU(2) phase $\exp(-i\theta\sigma_x)\exp(i\theta\sigma_y)$ is acquired. On the other hand, when it hops from (i, j) to $(i, j + \hat{y})$ to $(i + \hat{x}, j + \hat{y})$, the phase it obtains is $\exp(i\theta\sigma_y)\exp(-i\theta\sigma_x)$. Therefore the interference between the two path along the plaquette becomes

$$(\exp(i\theta\sigma_y)\exp(-i\theta\sigma_x))^\dagger \exp(-i\theta\sigma_x)\exp(i\theta\sigma_y) = \exp(i\theta\sigma_x)\exp(-i\theta\sigma_y)\exp(-i\theta\sigma_x)\exp(i\theta\sigma_y). \quad (10)$$

This can be evaluated on the basis of Campbell–Hausdorff formula,

$$\exp(\theta X)\exp(\theta Y) = \exp\left(\theta(X + Y) + \frac{\theta^2}{2}[X, Y] + O(\theta^3)\right), \quad (11)$$

to find

$$\begin{aligned} & \exp(i\theta\sigma_x)\exp(-i\theta\sigma_y)\exp(-i\theta\sigma_x)\exp(i\theta\sigma_y) \\ & \approx \exp(i(\sigma_x - \sigma_y) + i\theta^2\sigma_z)\exp(-i\theta\sigma_x)\exp(i\theta\sigma_y) \\ & \approx \exp(i(\sigma_x - \sigma_y - \sigma_x) + 2i\theta^2\sigma_z)\exp(i\theta\sigma_y) \\ & \approx \exp(2i\theta^2\sigma_z), \end{aligned} \quad (12)$$

where we have dropped terms higher than θ^2 . Using the relation,

$$2\pi Ba^2/(h/e) = 2\theta^2\sigma_z, \quad (13)$$

we have [24, 25]

$$B = \frac{\hbar}{e} \frac{2\theta^2}{a^2} \sigma_z. \quad (14)$$

We now discuss the condition for the high polarization in terms of this spin dependent Lorentz force. We use Eq.(14) to estimate the strength of magnetic field

$$\bar{B}(\theta) = \frac{4}{\pi} \frac{\hbar}{e} \left(\frac{\theta}{a} \right)^2. \quad (15)$$

where we have averaged σ_z to be $2/\pi$, since the variation of the expectation value of σ_z is described by the cos–function. Since the kinetic energy is comparable to the confinement energy in single-channel transport, the velocity of an injected electron can be assumed to be

$$v \simeq \frac{\hbar}{m^*} \frac{\pi}{N_w}. \quad (16)$$

Then the corresponding cyclotron diameter is given by

$$2l_{\bar{B}}(\theta) = \frac{2m^*v}{e\bar{B}(\theta)} = \frac{2L_{\text{so}}^2}{N_w}. \quad (17)$$

The cyclotron diameter becomes shorter than the wire width ($2l_{\bar{B}}(\theta) < N_w$) if the spin precession length becomes shorter than the wire width ($L_{\text{so}} < N_w/\sqrt{2}$). As a result, electrons with opposite z –component spin are almost completely separated at the junction and nearly perfect spin polarization is obtained (Fig.6). This situation is similar to the mesoscopic cross junction in magnetic fields [26].

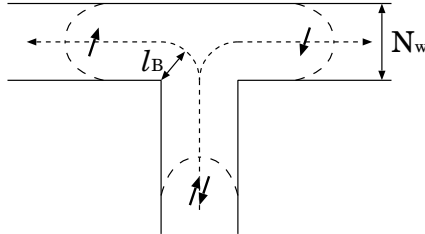


FIG. 6: Schematic view of the electron trajectory. A pair of the electrons with anti-parallel spins are almost completely separated at the junction when the cyclotron diameter becomes shorter than the wire width ($2l_{\bar{B}}(\theta) < N_w$).

B. The influence of disorder

We now consider briefly the effect of disorder on the spin polarization (Fig.7). An ensemble average is performed over 10^4 samples. The suppression of the polarization by disorder

becomes more prominent as the spin-orbit coupling becomes stronger. The mean free path of a 2DES in the tight-binding model is described by [22]

$$L_m = 48aV_0^{3/2} \frac{\sqrt{E + 4V_0}}{W^2}. \quad (18)$$

One can use this estimate to distinguish the ballistic regime from the diffusive one. For the present system, we obtain $W \simeq 1.53V_0$ for $L_m = 50a$ (indicated by an arrow in Fig. 7). As seen in the figure, the sample size must be smaller than the mean free path in order to obtain high spin polarization.

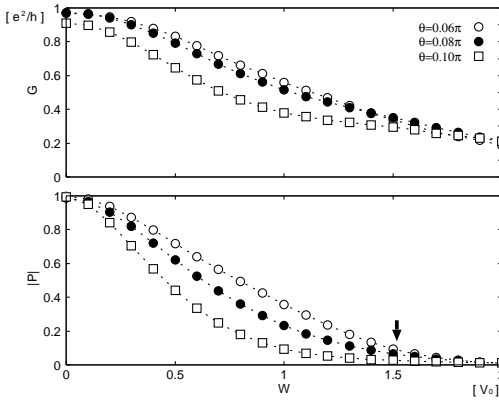


FIG. 7: Conductance G and spin polarization $|P|$ as functions of the strength of disorder W for several spin-orbit couplings at $E = -3.8V_0$. Ensemble average has been taken over 10^4 samples. For stronger spin-orbit coupling, the polarization becomes more sensitive to disorder. Arrow: crossover between ballistic and diffusive regimes [cf. Eq.(18)].

C. The influence of other channels

Finally let us consider the system whose size is $N_w = 50a$ and $N_l = 50a$. Figure 8 shows the dependence of the conductance and the spin polarization on the Fermi energy E for $\theta = 0.01\pi$. In this energy region where the number of channels increases to values ranging from 5 to 10, several channels contribute to transport. While the spin polarization is reduced by channel mixing, it still stays higher than 10%.

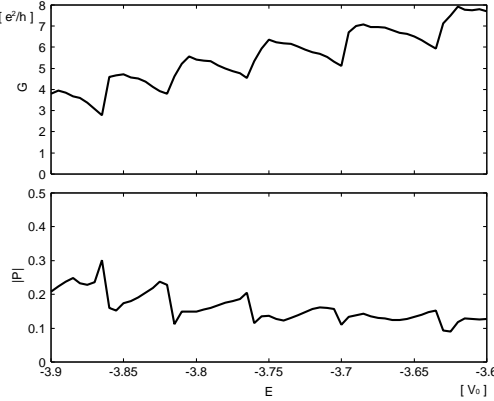


FIG. 8: Conductance G and spin polarization $|P|$ as functions of the Fermi energy E in the region of multi-channel transport. The system size is set to be $N_w = 50a$ and $N_l = 50a$, and the strength of spin-orbit coupling $\theta = 0.01\pi$. The number of channel increases to values ranging from 5 to 10 in this energy region. The polarization stays higher than 10%.

V. SUMMARY

In this paper we have investigated numerically spin polarized linear transport in a T-shaped conductor with Rashba spin-orbit coupling. We have considered single-channel transport and found that the spin polarization becomes almost perfect with a conductance close to G_0 for stronger spin-orbit coupling. Since the spin-orbit coupling can be regarded as the spin-dependent effective magnetic field [23], the propagating electrons with certain initial spin states are deflected into one of the two output terminals by Lorentz force while those with opposite spin states are deflected into the other. The ratio between the cyclotron diameter in an effective field and the wire width depends on that between the π -phase spin precession length and the wire width. If the precession length becomes shorter than the wire width, the cyclotron diameter becomes shorter than the wire width so that electrons with antiparallel spins are almost completely separated at the junction and nearly 100% polarization can be achieved.

With respect to the intrinsic spin Hall effect [27], we should note the following point. The spin-orbit induced effective magnetic field can cause the anomalous Hall effect in ferromagnets, where the spin direction of conduction electrons is maintained by the interaction between localized spin states. However, it can not simply separate injected electrons with up and down spins parallel to the z -axis in the investigated system since the spin states of

propagating electrons are always changing due to the spin precession [25].

We have also investigated the effect of disorder on the polarization. Since the polarization becomes more sensitive to the disorder when the spin-orbit interaction is stronger, one needs to prepare the clean samples so that the system belongs to the ballistic regime to realize the perfect polarization of the current.

In order to obtain information whether or not the predicted effects are observable in experiment, let us consider the parameters required for one of the favorable materials, InAs, with an effective mass $m^* = 0.039m_0$ (m_0 is the free electron mass) and Rashba coupling $\alpha = 23.8 \times 10^{-12}$ eVm [28]. Let us assume that the width of the conduction band is $\Delta = 1$ eV. This gives for $V_0 = \Delta/2Z = 125$ meV ($Z = 4$ for square lattice), and for the tight-binding lattice parameter $a = \hbar/(2m^*V_0)^{1/2} \simeq 2.8$ nm. Using the above numerical value of α one obtains $\theta = \alpha/2V_0a \simeq 0.01\pi$. This would reduce the polarization to about 10%, still a reasonable value for being observable in experiment. The crucial point, however, is the condition that the transport has to be in the single-channel regime. The wire width should be about 20 nm for single-channel transport when Fermi energy is of the order of 10 meV. In principle it is possible to fabricate such a narrow wire, but it makes the mean free path shorter and the effect of disorder may become critical. On the other hand, the wire width becomes 140 nm for the system with $N_w = 50a$ (Sec.IV C). This width of quantum wire can be easily fabricated than that for single-channel transport, which indicates that we can observe the spin polarization experimentally.

Acknowledgments

We thank J. Nitta, J. Ohe, K. Dittmer, K. Slevin and S. Murakami for fruitful discussions. This work was supported by SFB 508 “Quantenmaterialien” of the Deutsche Forschungsgemeinschaft, the Marie-Curie Network MCRTN-CT2003-504574 of the EU, and the Grant-in-Aid 14540363 from the Ministry of Education, Culture, Sports, Science and Technology.

APPENDIX A: RECURSIVE GREEN FUNCTION METHOD FOR MULTI-TERMINAL GEOMETRY

For numerical calculations, we apply the recursive Green function method [22] to the case of multi-terminal geometry. Let us consider three terminal geometry described in Fig.9. The central sample region (C) is attached to three probes (D , R and L). Each probe consists of the infinite ideal region and the sample one whose size is $N_p \times N_w^I$ ($I = D, R$ and L).

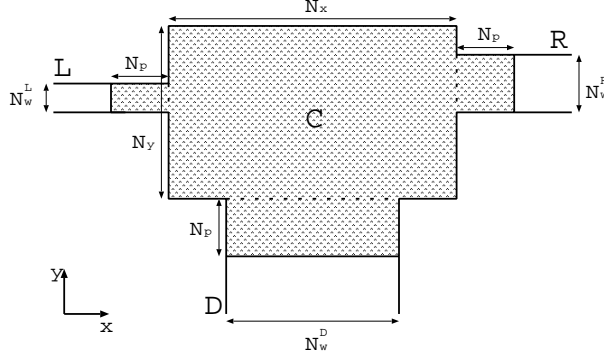


FIG. 9: Schematic draw of three terminal geometry. The shaded area represents a sample region where spin-orbit interaction is present. This sample region is connected to three electron reservoirs by ideal probes.

The full Hamiltonian can be written down as

$$\tilde{\mathcal{H}} = \begin{pmatrix} \tilde{\mathcal{H}}_{N_p+1} & -V_{N_p+1,N_p} & 0 & \cdots & 0 & 0 & 0 \\ -V_{N_p+1,N_p}^\dagger & \mathcal{H}_{N_p} & -V_{N_p,N_p-1} & \cdots & 0 & 0 & 0 \\ 0 & -V_{N_p,N_p-1}^\dagger & \mathcal{H}_{N_p-1} & \cdots & 0 & 0 & 0 \\ \vdots & \vdots & \vdots & \ddots & \vdots & \vdots & \vdots \\ 0 & 0 & 0 & \cdots & \mathcal{H}_2 & -V_{2,1} & 0 \\ 0 & 0 & 0 & \cdots & -V_{2,1}^\dagger & \mathcal{H}_1 & -V_{1,C}' \\ 0 & 0 & 0 & \cdots & 0 & -V_{1,C}^{\prime\dagger} & \mathcal{H}^C \end{pmatrix}. \quad (A1)$$

\mathcal{H}^C is the Hamiltonian for the central sample region and can be described by

$$\mathcal{H}^C = \begin{pmatrix} \mathcal{H}_1^C & -V_{12}^C & 0 & \cdots & 0 \\ -V_{21}^C & \mathcal{H}_2^C & -V_{23}^C & \cdots & 0 \\ 0 & -V_{32}^C & \mathcal{H}_3^C & \cdots & 0 \\ \vdots & \vdots & \vdots & \ddots & \vdots \\ 0 & 0 & 0 & \cdots & \mathcal{H}_{N_x}^C \end{pmatrix}, \quad (\text{A2})$$

where \mathcal{H}_i^C denotes the Hamiltonian for the i -th slice along the y -direction and V_{ij}^C the hopping term between the slice i and j . The hopping is restricted to nearest neighbours. $V'_{1,C}$ is the hopping term between the central sample region and its neighbouring slices of three probes. \mathcal{H}_i is the Hamiltonian for the set of i -th slices of three probes and can be described by

$$\mathcal{H}_i = \begin{pmatrix} \mathcal{H}_i^D & 0 & 0 \\ 0 & \mathcal{H}_i^R & 0 \\ 0 & 0 & \mathcal{H}_i^L \end{pmatrix}, \quad (\text{A3})$$

where \mathcal{H}_i^I ($I = D, R$ and L) is the Hamiltonian for the i -th slice of the probe I (see Fig.10). V_{ij} is the hopping term between the set of i -th slices and j -th ones.

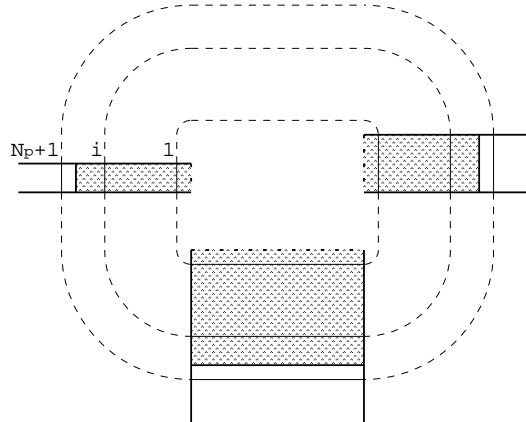


FIG. 10: Graphical interpretation for the Hamiltonian \mathcal{H}_i . The i -th slices of three probes are gathered.

Let us define some variables by following Ref.[22] as

$$\Lambda^I = \begin{pmatrix} \lambda_1^I & & \\ & \ddots & \\ & & \lambda_{N_w^I}^I \end{pmatrix}, \quad (\text{A4})$$

and

$$U^I = \left(\mathbf{u}_1^I \cdots \mathbf{u}_{N_w^I}^I \right), \quad (\text{A5})$$

where $\lambda_1^I, \dots, \lambda_{N_w^I}^I$ are the eigenvalues of transfer matrix for the ideal region on the probe I and $\mathbf{u}_1^I, \dots, \mathbf{u}_{N_w^I}^I$ the eigenfunctions corresponding to $\lambda_1^I, \dots, \lambda_{N_w^I}^I$. We note that the incoming solutions and outgoing ones have the same form when there is no magnetic field. Then the effective Hamiltonian on site $N_p + 1$ for the probe I can be written by

$$\tilde{\mathcal{H}}_{N_p+1}^I = \mathcal{H}_{N_p+1}^I - V_0 F^I, \quad (\text{A6})$$

with

$$F^I = U^I \Lambda^I (U^I)^{-1}, \quad (\text{A7})$$

where V_0 is the hopping term in the ideal probe. $\tilde{\mathcal{H}}_{N_p+1}$ can be obtained by exchanging \mathcal{H}_i^I for $\tilde{\mathcal{H}}_i^I$ in Eq.(A3) and setting $i = N_p + 1$.

We define corresponding Green function as

$$\hat{G} \equiv \frac{1}{E - \tilde{\mathcal{H}}} = \begin{pmatrix} \hat{G}_{N_p+1, N_p+1} & \hat{G}_{N_p+1, N_p} & \cdots & \hat{G}_{N_p+1, 1} & \hat{G}_{N_p+1, C} \\ \hat{G}_{N_p, N_p+1} & \hat{G}_{N_p, N_p} & \cdots & \hat{G}_{N_p, 1} & \hat{G}_{N_p, C} \\ \vdots & \vdots & \ddots & \vdots & \vdots \\ \hat{G}_{1, N_p+1} & \hat{G}_{1, N_p} & \cdots & \hat{G}_{1, 1} & \hat{G}_{1, C} \\ \hat{G}_{C, N_p+1} & \hat{G}_{C, N_p} & \cdots & \hat{G}_{C, 1} & \hat{G}_{C, C} \end{pmatrix}. \quad (\text{A8})$$

In principle, we can obtain Green function by the direct inversion of the matrix $E - \tilde{\mathcal{H}}$. However, the number of numerical operations required for the inversion of the matrix increases as N^3 with N the size of the matrix. We therefore need to reduce the size of matrix to inverse as small as possible.

Since we put the effective Hamiltonian $\tilde{\mathcal{H}}_{N_p+1}$ on the upper-left corner of the full Hamiltonian (Eq.(A1)), the sub-matrix \hat{G}_{N_p+1, N_p+1} contains all information of the transport. This sub-matrix can be calculated as

$$\hat{G}_{N_p+1, N_p+1} = \frac{1}{E - \tilde{\mathcal{H}}_{N_p+1} - \Gamma_{N_p+1}}, \quad (\text{A9})$$

where

$$\Gamma_{i+1} = V_{i+1, i} \frac{1}{E - \mathcal{H}_i - \Gamma_i} V_{i+1, i}^\dagger \quad (\text{for } i = 1, 2, \dots, N_p), \quad (\text{A10})$$

with

$$\Gamma_1 = V_{1, C}' \frac{1}{E - \mathcal{H}^C} V_{1, C}'^\dagger. \quad (\text{A11})$$

The inverse matrix of $E - \mathcal{H}^C$ can be calculated recursively[22] and each row of the matrix $V'_{1,C}$ contains only one non-zero element corresponding to the matrix element between neighbouring slices, which greatly simplifies the calculation of Γ_1 . In the calculation of Γ_{i+1} for $i = 1, 2, \dots, N_p$ and \hat{G}_{N_p+1, N_p+1} , we need to inverse directly the matrix whose size is $(N_w^D + N_w^R + N_w^L) \times (N_w^D + N_w^R + N_w^L)$. This is much smaller than the original size of $E - \tilde{\mathcal{H}}$. \hat{G}_{N_p+1, N_p+1} consists of 9 parts.

$$\hat{G}_{N_p+1, N_p+1} = \begin{pmatrix} \hat{G}^{DD} & \hat{G}^{DR} & \hat{G}^{DL} \\ \hat{G}^{RD} & \hat{G}^{RR} & \hat{G}^{RL} \\ \hat{G}^{LD} & \hat{G}^{LR} & \hat{G}^{LL} \end{pmatrix} \quad (\text{A12})$$

where \hat{G}^{IJ} ($I, J = D, R$ and L) is the Green function from the probe J to I . The scattering matrix can be calculated easily from the Green function [22].

- [1] S.A. Wolf *et al.*, Science **294**, 1488 (2001).
- [2] I. Zutic, J. Fabian and S.D. Sarma, Rev. Mod. Phys. **76**, 323 (2004).
- [3] G. Dresselhaus, Phys. Rev. **100**, 580 (1955).
- [4] E.I. Rashba, Sov. Phys. Solid State **2**, 1109 (1960).
- [5] Y.A. Bychkov and E.I. Rashba, J. Phys. C **17**, 6039 (1984).
- [6] G. Lommer, F. Malcher and U. Rössler, Phys. Rev. Lett. **60**, 728 (1988).
- [7] J. Nitta, T. Akazaki, H. Takayanagi and T. Enoki, Phys. Rev. Lett. **78**, 1335 (1997).
- [8] G. Engels, J. Lange, Th. Schäpers and H. Lüth, Phys. Rev. B **55**, R1958 (1997).
- [9] S. Datta and B. Das, Appl. Phys. Lett. **56**, 665 (1990).
- [10] G. Schmidt, D. Ferrand, L.W. Molenkamp, A.T. Filip and B.J. van Wees, Phys. Rev. B **62**, R4790 (2000).
- [11] L.D. Landau and E.M. Lifshitz, *Quantum mechanics: non-relativistic theory*, 3d ed., Pergamon Press, New York, (1991).
- [12] A.A. Kiselev and K.W. Kim, Appl. Phys. Lett. **78**, 775 (2001).
- [13] A.A. Kiselev and K.W. Kim, J. Appl. Phys. **94**, 4001 (2003).
- [14] M. Governale and U. Zülicke, Phys. Rev. B **66**, 073311 (2002).
- [15] C.W.J. Beenakker, Rev. Mod. Phys. **69**, 731 (1997).
- [16] A.G. Mal'shukov and K.A. Chao, Phys. Rev. B **61**, R2413 (2000).

- [17] A.A. Kiselev and K.W. Kim, Phys. Rev. B **61**, 13115 (2000).
- [18] B.K. Nikolić and S. Souma, Phys. Rev. B **71**, 195328 (2005).
- [19] S. Pramanik, S. Bandyopadhyay and M. Cahay, cond-mat/0403021.
- [20] T. Ando, Phys. Rev. B **40**, 5325 (1989).
- [21] R. Landauer, IBM J. Res. Dev. **1**, 223 (1957).
- [22] T. Ando, Phys. Rev. B **44**, 8017 (1991).
- [23] R. Karplus and J. Luttinger, Phys. Rev. **95**, 1154 (1954).
- [24] J. Li, L. Hu and S.-Q. Shen, cond-mat/0502102.
- [25] B.K. Nikolić, L.P. Zárbo and S. Welack, cond-mat/0503415, to appear in Phys. Rev. B.
- [26] C.W.J. Beenakker and H. van Houten, Phys. Rev. Lett. **63**, 1857 (1989).
- [27] S. Murakami, N. Nagaosa and S.-C. Zhang, Science **301**, 1348 (2003).
- [28] C.-M. Hu, C. Zehnder, Ch. Heyn and D. Heitmann, Phys. Rev. B **67**, 201302(R) (2003).